International Journal of Scientific Research in Mathematical and Statistical Sciences
Volume-8, Issue-5, pp.06-20, October (2021)

Research Paper

E-ISSN: 2348-4519

Mixed Convection Boundary Layer Flow with Heat Transfer over a Non-Linear Stretching Wedge-Shaped Surface with the Correlation Coefficient and Multiple Regressions Models

M. Ali [1*], M.A. Alim[2]

[1]Dept. of Mathematics, Chittagong University of Engineering and Technology, Chittagong, Bangladesh
[2]Dept. Mathematics, Bangladesh University of Engineering and Technology, Dhaka, Bangladesh

[*]*Corresponding Author: ali.mehidi93@gmail.com, Tel.: +88-01713109929*

Available online at: www.isroset.org

Received: 15/Aug/2021, Accepted: 28/Sept/2021, Online: 31/Oct/2021

Abstract— The present paper aims to investigate the MHD two-dimensional mixed convection boundary layer nanofluid flow and heat transfer along with a power-law stretching wedge-shaped surface by using the Buongiorno model. The leading PDEs are modified to ODEs by applying the appropriate similarity transformation. The mathematical model of this problem is solved with the help of SQLM along with MATLAB. Numerical solutions of fluid velocity profile and fluid temperature profile are displayed graphically for different values of controlling flow parameters whereas numerical values of velocity gradient and wall temperature gradient are presented in a tabular form. The numerical results of this paper have been compared with previous working results and found to be almost similar. The correlation coefficient and multiple regression model have been established for the mentioned parameters. The correlation analysis represents that the stretching ratio parameter is negatively correlated with the velocity gradient but the magnetic parameter, porosity parameter, mixed convection parameter and suction parameter are positively correlated. The temperature gradient is positively correlated with the Prandtl number, stretching ratio parameter, porosity parameter, magnetic parameter, and suction parameter whereas negatively correlated with Brownian motion, thermophoresis parameter, and heat generation parameter. The concentration gradient is positively correlated with the Brownian motion, Lewis number, Prandtl number, heat generation, and suction parameter but negatively correlated with the thermophoresis parameter, magnetic parameter and porosity parameter. The results also indicate that within the boundary layer region the fluid velocity is a decreasing function of wedge angle parameter, magnetic parameter, and increasing function of stretching ratio, porosity, wedge angle and mixed convection parameters. Similarly, the temperature is an increasing function of heat generation parameter, Brownian motion, and thermophoresis parameter but a decreasing function of Prandtl number and suction parameter whereas constant in the case of mixed convection parameter. Again, the concentration is a decreasing function of Prandtl number, Lewis number, Brownian motion, heat generation and suction parameter but an increasing function thermophoresis parameter. The observation of this problem may have a bearing in different engineering techniques such as the paper industry, annealing, and tinning of copper wire industry, the process of crystal growing and glass blowing, the continual casting of metals, and spinning of fibbers.

Keywords—Boundary layer, wedge flow, correlation, regression, Mixed convection

I. INTRODUCTION

The analysis of boundary layer flow over a stretching surface is an important problem in many engineering technologies with applications in industrial sectors. Such situations hold in polymer dispensation, making of glass sheets, paper production, wire drawing, hot rolling, fibre production, polymer processing, atmospheric flow, biomedical devices, solar energy storage, heat exchanger, drying technology, cooling of the electronic device, etc. The wedge is a triangular-shaped geometry that can be used in the system of the two separate objects. The lateral force converts into a transverse splitting force by the wedge. Therefore, the wedge-shaped geometry is helpful to hold the gate valves in the engine because it is the mechanism that opens by lifting the wedge-shaped disc as a result, its control of the timing and quantity of fluid flow into an engine. Falkner and Skan were firstly developed a viscous fluid flow model in the case of a static wedge by using similarity transformation that can be used to reduce the partial differential equation of the boundary layer equations to a nonlinear third-order ordinary differential equation [1]. This equation was first analysed on the boundary layer flow by applying the stream-wise pressure gradient. In the past few decades, a lot of research work has been done on Falkner-Skan flow by considering various parameter effects. Nagendramma et al. investigated the effect of magnetic and viscous dissipation on velocity and temperature fields by considering the stretching wedge and observed that the flow separation occurs for the small values of unsteady and wedge angle parameters [3]. Ashwini et al. analysed the unsteady MHD BL flow over a

wedge with the help of heat generation and thermal radiation [4]. Ramesh et al. studied the magnetohydrodynamic BL flow over a constant wedge through porous media [5]. It is observed that the thickness of the boundary layer reduces for positive values of pressure gradient and mass transfer but negative values have different solutions. Ibrahim analysed the effect of the viscous dissipation, Brownian motion, and thermophoresis on MHD boundary layer nanofluid flow over a wedge through porous media [6]. The author observed that the thickness of the velocity boundary layer decreases for increasing pressure gradient, permeability, and magnetic parameters, but thermal BL thickness increases for larger values of Eckert number, Brownian motion, and thermophoresis parameters. Nageeb et al. studied the free and forced convection boundary layer nanofluid flow with heat transfer over a stretching sheet with a magnetic effect [7]. Kashmani et al. discussed the influence of the soret and Dufour effect on the boundary layer nanofluid flow and heat transfer over a moving wedge [8]. It is seen that the heat transfer rate enhances for soret number and decreases for Dufour number whereas the opposite trends are observed in mass transfer rate. Waini et al. discussed the MHD BL hybrid nanofluid flow and heat transfer over a permeable stretching/shrinking wedge and found that the hybrid nanofluid increases the heat transfer rate than regular nanofluid [9]. Rajab Al-Sayagh studied the free convective heat transfer by using a U-shaped obstacle in an Al_2O_3-water nanofluid [10]. Khan and Pop examined the boundary layer nanofluid flow with heat transfer over a wedge [12]. Younes Menni et al. presented the boundary layer flow and heat transfer of water, ethylene glycol and water-ethylene glycol based nanofluid dispersed by aluminum oxide nano-sized solid particles [14]. Khan et al. analysed the MHD boundary layer flow and heat, mass transfer over a vertical stretching/shrinking sheet in the presence of suction, chemical reaction, and heat source effects of a double stratified micropolar fluid [15]. It is observed that the reduced skin friction coefficient and the Nusselt number enhance with the enhancing chemical reaction and heat source parameters. The higher values of the chemical reaction parameter have increased the magnitude of the local Sherwood number. Yusof et al. studied the boundary layer stagnation point flow and radiative heat transfer of a non-Newtonian fluid over an exponentially permeable slippery Riga plate with thermal radiation, magnetic field, velocity slip, thermal slip, and viscous dissipation effects [16]. It is noticed that the velocity boundary layer thickness expands with increasing values of the casson parameter. The temperature decreases within the boundary layer region due to the velocity slip parameter and thermal slip parameter. Ewis et al. investigated the effects of variable thermal conductivity, porosity, and Grashof number on natural convection boundary layer flow with heat transfer [17]. It is seen that the skin friction coefficient enhances with rising the thermal conductivity parameter but reduces the Nusselt number. Nyakebogo et al. examined the unsteady MHD boundary layer flow along a vertical stretching surface by using the FTCS scheme [18]. It is noticed that the Forward Time Centered Space scheme is conditionally applicable for both equations. Rahul Mehta and Kataria studied the unsteady natural convection magnetohydrodynamic boundary layer flow over an oscillating vertical surface by the influence of the heat generation/absorption, thermal radiation, and chemical reaction parameters [19]. Wilfred Samuel Raj and Anjali Devi investigated the nonlinear radiation effects on magnetohydrodynamic boundary layer flow and heat transfer over a shrinking sheet with heat generation and viscous dissipation [20].

Hence, the present research work focuses on MHD boundary layer nanofluid flow over the stretching wedge-shaped surface by using the Buongiorno model with SQLM. So, the velocity profile, energy profile, and concentration profile in addition to the skin friction and heat transfer properties have been discussed graphically and also through correlation coefficient by the numerical data. Therefore, the main objective of the present work is to determine the effects of the controlling parameters on the velocity field, temperature field, concentration field, skin friction, Nusselt number, and Sherwood number and also developed a relationship between the mentioned parameters and fluid flow properties by using the correlation coefficient and multiple regressions.

II. FLOW ANALYSIS

Let us consider that u_w is the surface velocity, U is the free stream velocity, T_w is the wall temperature T_∞ is the free stream temperature, u and v are velocity components of the x and y-coordinates respectively. Figure 1 describes the physical model and coordinate system. From this figure, $\Omega = \beta\pi$ is the total wedge angle and β is the wedge angle parameter.

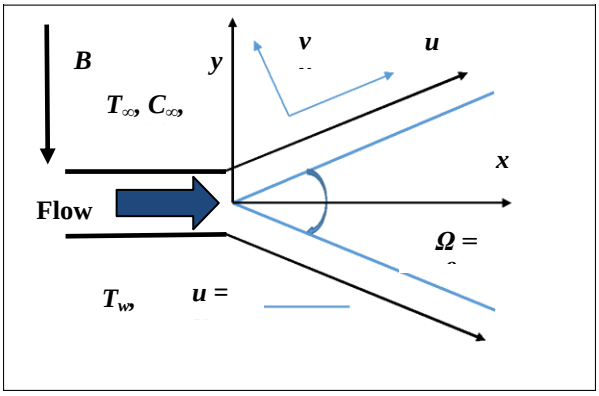

Figure 1. Geometrical configuration and coordinate system

The PDEs of the boundary layer nanofluid flow are as follows [11]:
Equation of continuity:

$$\frac{\partial u}{\partial x}+\frac{\partial v}{\partial y}=0 \qquad (1)$$

Momentum equation:

$$u\frac{\partial u}{\partial x}+v\frac{\partial u}{\partial y}=U\frac{dU}{dx}+\nu\frac{\partial^2 u}{\partial y^2}+\left(\frac{\sigma B_0^2}{\rho}+\frac{\nu}{K}\right)(U-u)+g\beta^*\left(T-T_\infty\right) \quad (2)$$

Energy equation:

$$u\frac{\partial T}{\partial x}+v\frac{\partial T}{\partial y}=\alpha\frac{\partial^2 T}{\partial y^2}+\frac{Q}{\rho c_p}\left(T-T_\infty\right)+\tau\left\{D_B\left(\frac{\partial T}{\partial y}\frac{\partial C}{\partial y}\right)+\frac{D_T}{T_\infty}\left(\frac{\partial T}{\partial y}\right)^2\right\} \quad (3)$$

Concentration equation:

$$u\frac{\partial C}{\partial x}+v\frac{\partial C}{\partial y}=D_B\frac{\partial^2 C}{\partial y^2}+\frac{D_T}{T_\infty}\frac{\partial^2 T}{\partial y^2} \quad (4)$$

The term $\frac{\sigma B_0^2}{\rho}u$ in equation (2) denotes the Lorentz force which arises from the interaction of the fluid velocity and the applied magnetic field. In equation (2) the induced magnetic field is neglected due to the smallest magnetic Reynolds number. This consideration is justified due to electrically conductive fluids such as mercury and liquid sodium. Equation (3) represents that heat can be transported in a fluid by convection, conduction, and also by nanoparticle diffusion. Hence in equation (3) the convection and conduction terms are $u\frac{\partial T}{\partial x}+v\frac{\partial T}{\partial r}$ and $\alpha\frac{\partial^2 T}{\partial r^2}$ respectively. The terms $\tau D_B\left(\frac{\partial T}{\partial y}\frac{\partial C}{\partial y}\right)$ and $\tau\frac{D_T}{T_\infty}\left(\frac{\partial T}{\partial y}\right)^2$ are the energy transport due to Brownian diffusion and thermophoretic effect.

The boundary conditions are:

$$u=u_w=ax^m,\quad v=-v_w,\quad T=T_w=T_\infty,\quad C=C_w=C_\infty,\ \text{at}\quad y=0$$
$$u=U=bx^m,\quad T=T_\infty,\quad C=C_\infty,\quad \text{at}\quad y=\infty$$

Here m is the power-law index parameter and is related to the wedge angle parameter β, $v_w=-\sqrt{\frac{\nu u_w}{x}}F_w$ is a special class of velocity in which $v_w(x)>0$ represents suction and $v_w(x)<0$ represents blowing.

For converting the governing equations (2) – (4), the following transformation has been considered:

$$\eta=y\sqrt{\frac{(1+m)u}{2x\nu}},\ \psi=\sqrt{\frac{2x\nu u}{(1+m)}}F(\eta),\ \theta(\eta)=\frac{T-T_\infty}{T_w-T_\infty},\ \varphi(\eta)=\frac{C-C_\infty}{C_w-C_\infty},$$
$$u=\frac{\partial\psi}{\partial y},\ \text{and}\ v=-\frac{\partial\psi}{\partial x}$$

After applying these similarity transformations, the transformed equations of momentum, energy, and concentration are:

$$F'''(\eta)+F(\eta)F''(\eta)+\beta\left(\varepsilon^2-F'^2(\eta)\right)+\left(\frac{M+K^*}{1+m}\right)\left(\varepsilon-F'(\eta)\right)+\lambda\theta(\eta)=0 \quad (5)$$

$$\theta''(\eta)+\Pr\left[\begin{matrix}F(\eta)\theta'(\eta)+Nb\theta'(\eta)\varphi'(\eta)\\+Nt\theta'^2(\eta)+Q^*\theta(\eta)\end{matrix}\right]=0 \quad (6)$$

$$\varphi''(\eta)+\frac{Nt}{Nb}\theta''(\eta)+Le\Pr F(\eta)\varphi'(\eta)=0 \quad (7)$$

The transformed boundary conditions:

$$F(\eta)=S,\quad F'(\eta)=1,\quad \theta(\eta)=1,\quad \varphi(\eta)=1\quad \text{at}\quad \eta=0$$
$$F'(\eta)\to\varepsilon,\quad \theta(\eta)=\varphi(\eta)\to 0,\quad \text{at}\quad \eta\to\infty$$

The prime means derivative with respect to η. The mathematical expression of M is the magnetic parameter, ϵ is the stretching ratio parameter, Pr is the Prandtl number, Nb is the Brownian motion parameter, β is the wedge angle parameter, Le is the Lewis number, K* is the permeability parameter, λ is the mixed convection parameter, Nt is the thermophoresis parameter, Re is the Reynold's number, Gr is the Grashof number, Q* is the heat generation parameter, S is the suction parameter respectively are written as:

$$M=\frac{2\sigma B_0^2 x}{\rho u},\ \varepsilon=\frac{b}{a},\ Pr=\frac{\nu}{\alpha},\quad \beta=\frac{2m}{1+m},$$
$$Nb=\frac{\tau D_B\left(C_w-C_\infty\right)}{\nu},Le=\frac{\nu}{D_B},\ S=-\sqrt{\frac{(1+m)\nu u}{x}}F(0)$$
$$\lambda=\frac{Gr}{\mathrm{Re}^2},Nt=\frac{\tau D_T\left(T_w-T_\infty\right)}{T_\infty\nu},\mathrm{Re}_x=\frac{u_w L}{\nu},K^*=\frac{2\nu x}{Ku},$$
$$Gr=\frac{g\beta\left(T_w-T_\infty\right)L^3}{\nu^2},Q^*=\frac{QL\left(T_w-T_\infty\right)}{\rho a c_p},$$

Now the skin friction coefficient C_F, local Nusselt number Nu_x, and local Sherwood number Sh_x are defined as:

$$\tau_w = \mu\left(\frac{\partial u}{\partial y}\right)_{y=0}, q_w = -k\left(\frac{\partial T}{\partial y}\right)_{y=0}, \text{ and } J_w = -D_B\left(\frac{\partial C}{\partial y}\right)_{y=0}$$

where τ_w, q_w and J_w are the shear stress, heat flux, and mass flux of the surfaces, respectively.
Therefore, the non-dimensional skin friction coefficient, local Nusselt number, and local Sherwood number can be written as:

$$C_F\left(\mathrm{Re}_x\right)^{\frac{1}{2}} = \sqrt{2(1+m)}F''(0), Nu_x\left(\mathrm{Re}_x\right)^{-\frac{1}{2}} = -\sqrt{\frac{(1+m)}{2}}\theta'(0),$$

$$Sh_x\left(\mathrm{Re}_x\right)^{-\frac{1}{2}} = -\sqrt{\frac{(1+m)}{2}}\varphi'(0)$$

III. METHODOLOGY

Bellman and Kalaba [13] were the first to apply the SQLM about half a century ago to solve nonlinear ODE and PDE. Since the differential equation is highly non-linear and it is almost impossible to find the closed-form analytic solution. Thus, for numerical calculation, we need to choose an appropriate numerical technique. The SQLM is a combination of two methods such as Quasi-linearization method (QLM) and the Chebyshev spectral collocation method. The QLM is used to linearize the non-linear ODEs into linear ODEs. The QLM approaches that the difference between the approximate solution at the present iteration and the previous iteration is very small. The quadratic convergence property is the advantage of this technique. Three to six iterations are needed for getting five-digit accuracy if the technique converges. The numerical simulation of the present problem is obtained with the help of SQLM which gives highly accurate results. Since the similarity variable are taken as $\eta \to \infty$ but the present simulation has been performed for a finite domain of $\eta = 5, 25 \text{ and } 10$ for velocity, temperature, and concentration profiles respectively. Therefore, the dimensionless velocity, energy, and concentration distribution within the boundary layer asymptotically tend to a free stream velocity to satisfy the boundary conditions. So, after applying the SQLM, the system of equations (5) - (7) are converted into the following iterative sequence of linear differential equations.

$$a_{0,r}\frac{\partial^3 F_{r+1}}{\partial\eta^3} + a_{1,r}\frac{\partial^2 F_{r+1}}{\partial\eta^2} + a_{2,r}\frac{\partial F_{r+1}}{\partial\eta} + a_{3,r}F_{r+1} + a_{4,r}\theta_{r+1} = R_{1,r}$$

$$b_{0,r}\frac{\partial^2\theta_{r+1}}{\partial\eta^2} + b_{1,r}\frac{\partial\theta_{r+1}}{\partial\eta} + b_{2,r}\theta_{r+1} + b_{3,r}\frac{\partial^2 F_{r+1}}{\partial\eta^2} + b_{4,r}\frac{\partial F_{r+1}}{\partial\eta} + b_{5,r}F_{r+1} = R_{2,r}$$

$$e_{0,r}\frac{\partial^2\varphi_{r+1}}{\partial\eta^2} + b_{1,r}\frac{\partial\varphi_{r+1}}{\partial\eta} + e_{2,r}\varphi_{r+1} + e_{3,r}\frac{\partial^2\theta_{r+1}}{\partial\eta^2} + e_{4,r}\frac{\partial F_{r+1}}{\partial\eta} + e_{5,r}F_{r+1} = R_{3,r}$$

Where the variable coefficients obtained from the previous iteration are given by

$$a_{0,r} = 1, a_{1,r} = F_r, a_{2,r} = -2\beta F_r' - \left(\frac{M+K^*}{1+m}\right), a_{3,r} = F_r'',$$

$$a_{4,r} = \lambda, b_{0,r} = 1, b_{1,r} = \mathrm{Pr}\left(F_r + Nb\varphi_r' + 2Nt\theta_r'\right),$$

$$b_{2,r} = \mathrm{Pr}\left(-\beta F_r' + Q^*\right), b_{3,r} = -\mathrm{Pr}\,\beta\theta_r, b_{4,r} = \mathrm{Pr}\,\theta_r',$$

$$b_{5,r} = \mathrm{Pr}\,Nb\theta_r', e_{0,r} = 1, e_{1,r} = Le\,\mathrm{Pr}\,F_r, e_{2,r} = -Le\,\mathrm{Pr}\,\beta F_r',$$

$$e_{3,r} = \frac{Nt}{Nb}, e_{4,r} = -Le\,\mathrm{Pr}\,\beta\varphi_r, e_{5,r} = Le\,\mathrm{Pr}\,\varphi_r'$$

The terms on the right are defined as follows

$$R_{1,r}(\eta) = a_{0,r}F_r''' + a_{1,r}F_r'' + a_{2,r}F_r' + a_{3,r}F_r + a_{4,r}\theta_r - G\left[\eta, F(\eta), F'(\eta), F''(\eta).....F^n(\eta)\right]$$
$$= F_rF_r'' - \beta\left(\varepsilon^2 - F_r'^2\right) - \varepsilon\left(\frac{M+K^*}{1+m}\right)$$

$$R_{2,r}(\eta) = b_{0,r}\theta_r'' + b_{1,r}\theta_r' + b_{2,r}\theta_r + b_{3,r}f_r'' + b_{4,r}f_r' + b_{5,r}f_r - G\left[\eta, F(\eta), F'(\eta), F''(\eta).....F^n(\eta)\right]$$
$$= \mathrm{Pr}\left[F_r\theta_r' - \beta F_r'\theta_r + Nb\theta_r'\varphi_r' + Nt\left(\theta_r'\right)^2\right]$$

$$R_{3,r}(\eta) = e_{0,r}\varphi_r'' + e_{1,r}\varphi_r' + e_{2,r}\varphi_r + e_{3,r}\theta_r'' + e_{4,r}F_r' + e_{5,r}F_r - G\left[\eta, F(\eta), F'(\eta), F''(\eta).....F^n(\eta)\right]$$
$$= Le\,\mathrm{Pr}\left(F_r\varphi_r' - \beta F_r'\varphi_r\right)$$

Evaluating Equations (8) - (10) for the collocation points and approximating derivatives with Chebyshev derivatives which provide in a vector-matrix form such as

$$\begin{bmatrix} A_{11} & A_{12} & A_{13} \\ A_{21} & A_{22} & A_{23} \\ A_{31} & A_{32} & A_{33} \end{bmatrix}\begin{bmatrix} F_{r+1} \\ \theta_{r+1} \\ \varphi_{r+1} \end{bmatrix} = \begin{bmatrix} R_{1,r} \\ R_{2,r} \\ R_{3,r} \end{bmatrix} \quad (8)$$

Were

$$A_{11} = a_{0,r}D^3 + a_{1,r}D^2 + a_{2,r}D + a_{3,r},$$

$$A_{12} = a_{4,r}, A_{13} = 0I, A_{2,1} = b_{3,r}D + b_{4,r},$$

$$A_{2,2} = b_{0,r}D^2 + b_{1,r}D + b_{2,r}, A_{23} = b_{5,r}D \quad (9)$$

$$A_{3,1} = e_{4,r}D + e_{5,r}, A_{3,2} = e_{3,r}D^2,$$

$$A_{3,3} = e_{0,r}D^2 + e_{1,r}D + e_{2,r}$$

The transformed boundary conditions

$$F_{r+1}(\eta_0) = F_w, F'_{r+1}(\eta_0) = 1, \theta_{r+1}(\eta_0) = 1,$$
$$\varphi_{r+1}(\eta_0) = 1, \mathrm{R}_r(\eta_N) = 1 \text{ at } \eta = 0$$
$$F_{r+1}(\eta_N) = F_w, F'_{r+1}(\eta_N) \to \varepsilon,$$
$$\theta_{r+1}(\eta_N) = \varphi_{r+1}(\eta_0) \to 0,$$
$$\mathrm{R}_r(\eta_{N+1}) \to \varepsilon \text{ as } \eta \to \infty$$

IV. RESULTS AND DISCUSSION

The non-linear ODEs of the present problem are solved by applying SQLM. The convergence criteria of the solution are performed by the use of solution-based errors. These errors are defined by the differences between approximate solutions at the previous and current iteration levels t and t + 1, respectively. The error norms are defined as:

$$Error_f = \max_{0 \le i \le N} \left\| F_{t+1,i} - F_{t,i} \right\| \text{ and}$$
$$Error_\theta = \max_{0 \le i \le N} \left\| \theta_{t+1,i} - \theta_{t,i} \right\|$$

The infinity norms of the residual errors are as

$$\left\| \mathrm{Res}(F) \right\|_\infty = \left\| \begin{matrix} F''' + FF'' + \beta\left(\varepsilon^2 - F'^2\right) + \\ \left(\frac{M + K^*}{1+m}\right)(\varepsilon - F') + \lambda\theta \end{matrix} \right\| = 0$$

$$\left\| \mathrm{Res}(\theta) \right\|_\infty = \left\| \theta'' + \mathrm{Pr}\left[\begin{matrix} F\theta' + Nb\theta'\varphi' + \\ Nt\theta'^2 + Q*\theta \end{matrix} \right] \right\| = 0$$

$$\left\| \mathrm{Res}(\varphi) \right\|_\infty = \left\| \varphi'' + \frac{Nt}{Nb}\theta'' + Le\,\mathrm{Pr}\,F\varphi' \right\| = 0$$

The impact of physical parameters on velocity $f'(\eta)$, temperature $\theta(\eta)$, and concentration $\varphi(\eta)$ has been shown graphically. The numerical values of skin friction ($C_f\sqrt{\mathrm{Re}_x}$), Nusselt number ($Nu_x\left(\sqrt{\mathrm{Re}_x}\right)^{-1}$), and Sherwood number ($Sh_x\left(\sqrt{\mathrm{Re}_x}\right)^{-1}$) which are equivalent to the rate of velocity $f''(0)$, rate of heat transfer $\theta'(0)$, and rate of concentration $\varphi'(0)$ respectively that have been shown in Table 1 and Table 2. The computations are done by taking N = 60 collocation points and solution-based errors are defined for the convergence of the numerical method. So, Figures 2(a) and 2(b) show the convergence and accuracy of the present problem. Figure 2(a) represents the infinity norms with iterations. The error infinity norm decreases with the increasing number of iterations that confirms the convergence of the present method. So, the present method converges after six iterations. Figure 2(b) represents the residual error norms of less than 10^{-1} for $f(\eta)$, $\theta(\eta)$ and $\varphi(\eta)$ against after third iterations. It is seen that the residual error reduces with enhancing the iterations. This proves the validity of the present method. The errors show that the SQLM is accurate giving errors of less than 10^{-1} within fifth iterations. Figure 2 shows the convergence and accuracy of the SQLM. We note that an enhance in the number of iterations results in a decrease of the error infinity norm and the method converges after six iterations. Also, the decrease in residual error infinity norms against the number of iterations confirms the accuracy of the numerical method. The SQLM achieves an accuracy of order 10^{-1} after third iterations and that confirms the accuracy of the method. The present numerical calculation has been performed by taking

$$0.0 \le M \le 15.0, 0.2 \le Nb \le 0.6, 0.2 \le Nt \le 0.6,$$
$$0.5 \le K^* \le 3.5, 0.1 \le \beta \le 0.4, 0.71 \le \mathrm{Pr} \le 10.0,$$
$$5.0 \le Le \le 15.0, 0.5 \le \lambda \le 3.5$$

The results have been shown graphically and also in the table in the following sub-sections.

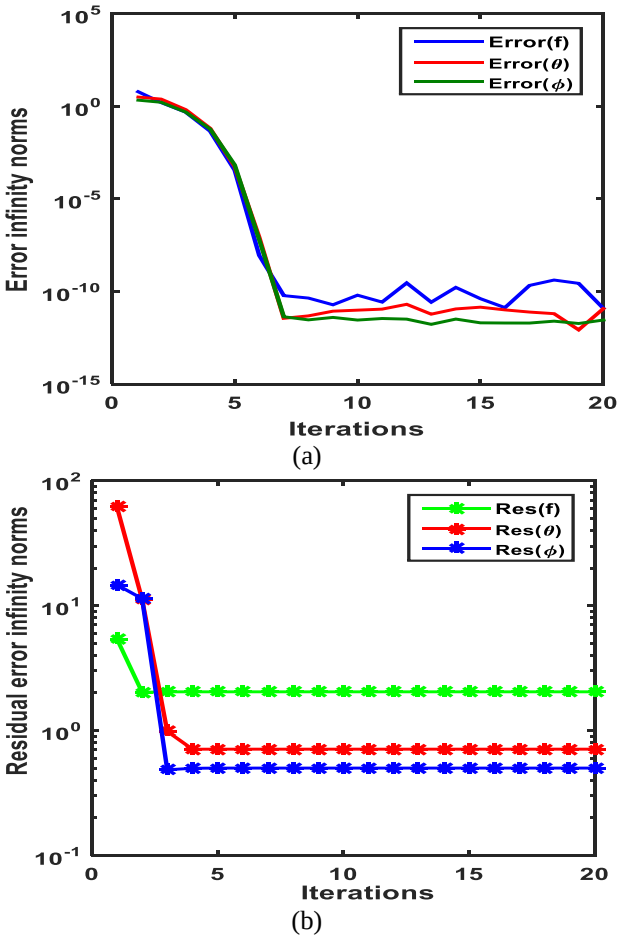

Figure 2. (a) Error infinity norms and (b) Residual error infinity norms for $f(\eta)$, $\theta(\eta)$ and $\varphi(\eta)$

V. VELOCITY PROFILE

Figures 3(a) – 3(f) display the influence of the magnetic parameter (M), stretching ratio parameter (ϵ), permeability parameter (K*), suction parameter (S), mixed convection parameter (λ), and wedge angle parameter (β) on the fluid velocity within the boundary layer region. These plots depict that the velocity profile of the viscous fluid and boundary layer thickness affected significantly with increasing magnetic parameter, stretching ratio parameter, permeability parameter, and suction parameter but insignificantly affected by increasing the mixed convection parameter and wedge angle parameter. The velocity profiles are expanding for increasing the stretching ratio parameter because the surface velocity increases. The increasing behaviour of the magnetic parameter increases the resistive forces that act against the fluid velocity which in turn decreases the fluid velocity and hence the motion of the fluid is slowed down. For increasing the suction parameter, the fluid towards close to the surface, which decreases the velocity profile as well as the momentum boundary layer. So that the fluid velocity can be controlled by suction or injection parameters. An increase in permeability parameter causes lower obstruction to the fluid flow, thus enhancing the fluid velocity into the boundary layer region. The physics of the parameter K* is that the higher the values of permeability causes higher resistance to the fluid motion as a result the velocity profiles decreases but in the present work the velocity profiles increases because the free stream velocity dominates the surface velocity. From Figure 3(e) it is seen that the fluid velocity enhances within the boundary layer region as the mixed convection parameter increases. This happens because the assisting flow (λ >0) induces a favorable pressure gradient which increases the fluid flow in the boundary layer and as a result, the velocity boundary layer expands. The physics of the wedge angle parameter is that increasing values of this parameter means to shape and size of the surface increases as a result the fluid velocity profiles increases. It can be concluded from this figure that the velocity distribution shows an increasing behavior for uplifting values of permeability parameter, stretching ratio parameter, wedge angle parameter, and mixed convection parameter, but a reverse trend has been found for the magnetic parameter, and suction parameter.

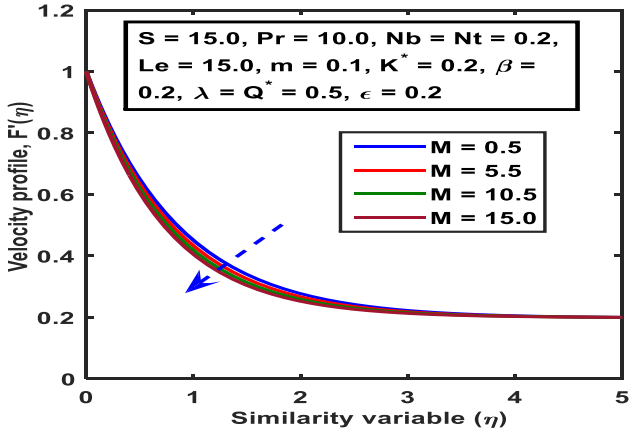

(a)

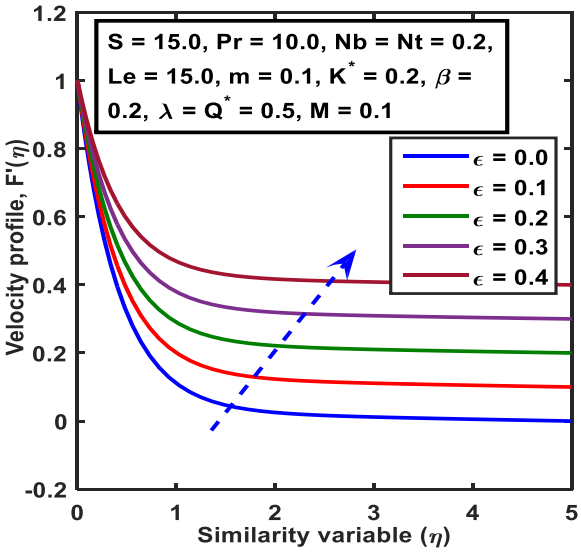

(b)

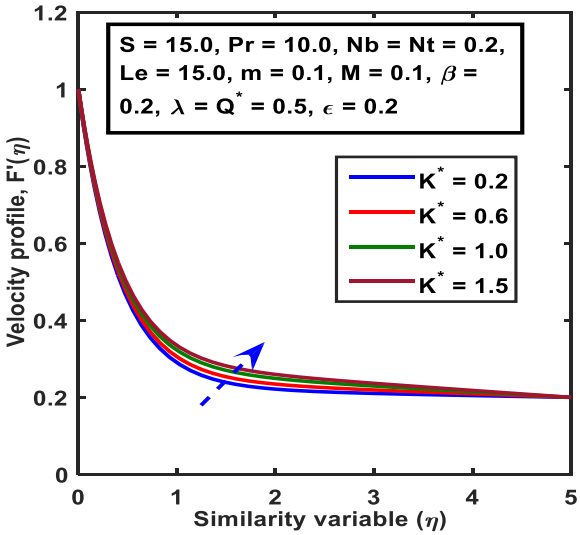

(c)

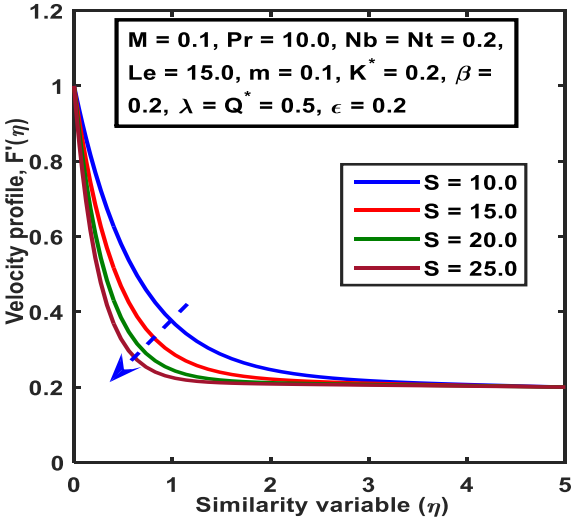

(d)

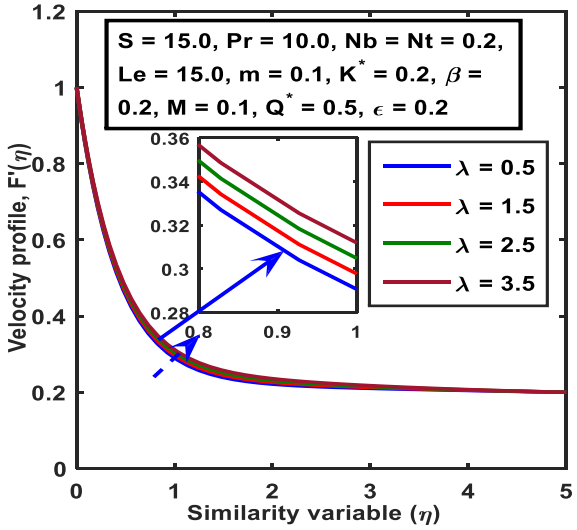

(e)

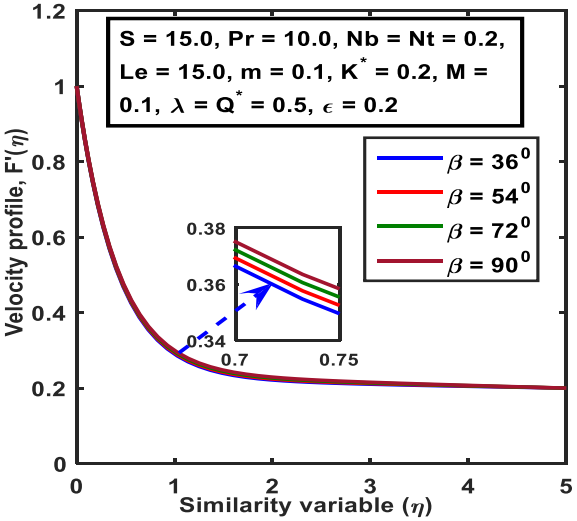

(f)

Figure 3. Velocity profile with η for the variation of (a) *M*, (b) ϵ, (c) *K** (d) S (e) λ and (f) β

VI. TEMPERATURE PROFILE

The temperature distribution for the variation of Prandtl number (Pr), Brownian motion (Nb), thermophoresis parameter (Nt), suction parameter, heat generation parameter (Q*), and mixed convection parameter (λ) have been displayed in figures 3(a–f). From these figures, it is observed that the temperature profiles and thermal boundary layer reduce by enhancing the values of Prandtl number and suction parameter whereas the reverse trend is observed for the Brownian motion, thermophoresis parameter, and heat generation parameter. On the other hand, the mixed convection parameter does not affect the temperature profile. These plots represent that the temperature profile of the viscous fluid and thermal boundary layer thickness affected significantly with increasing Prandtl number, thermophoresis parameter, suction parameter, and heat generation parameter but insignificantly effected by the Brownian motion and mixed convection parameter. In the case of a smaller Prandtl number heat is quickly diffuse from the heated surface than for higher values of Pr. For increasing values of Prandtl number, the temperature profiles are closing to the solid surface. So, for cooling purposes, the Prandtl number can be used. The temperature profile increases for increasing values of Brownian motion parameter because the fluid nanoparticles are moving randomly which accelerates the collision between nanoparticles and fluid molecules. Therefore, the kinetic energy of these molecules is converted into thermal energy within the boundary layer as a result the temperature profiles increases. The thermophoresis parameter and heat source parameter also increase the temperature profiles because thermophoresis accelerates the fluid particles from a hotter area to a cooler area as a result heat moves quickly from the hotter surface to the surrounding fluid and increases the temperature within the boundary layer. Due to the suction parameter more are stored in the boundary layer region as result, the temperature increases.

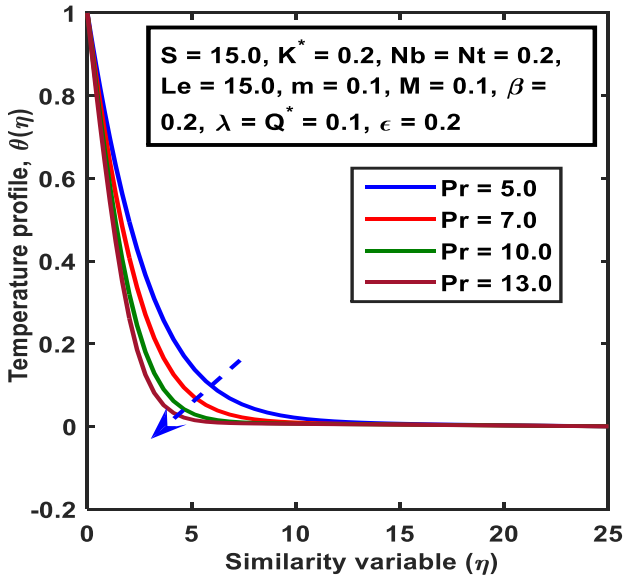

(a)

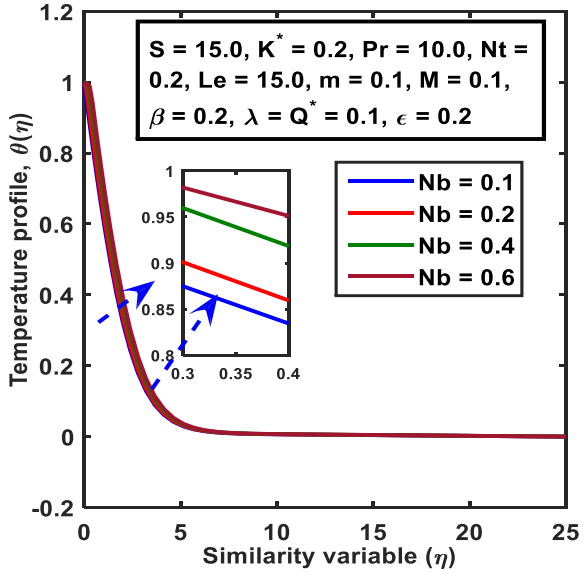

(b)

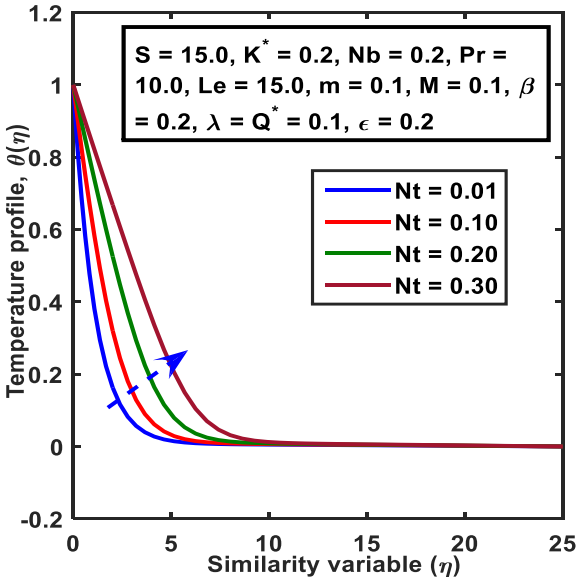

(c)

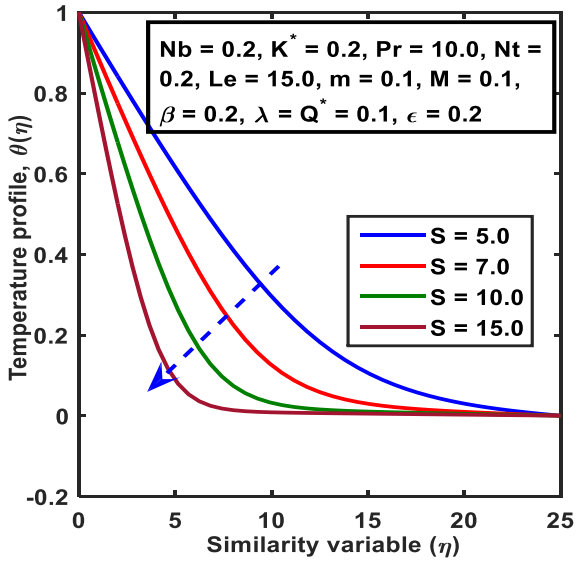

(d)

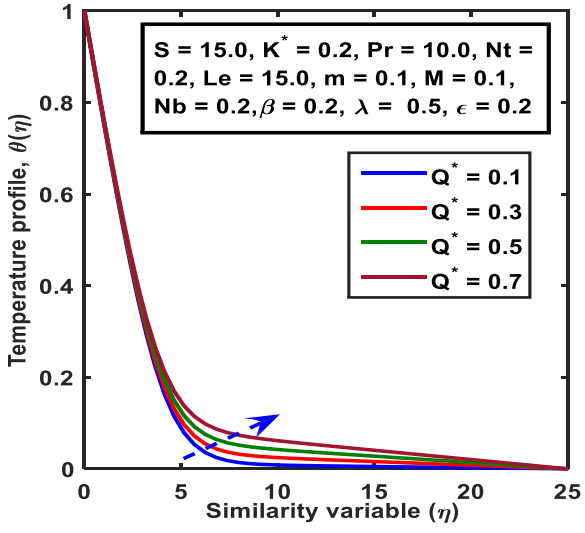

(e)

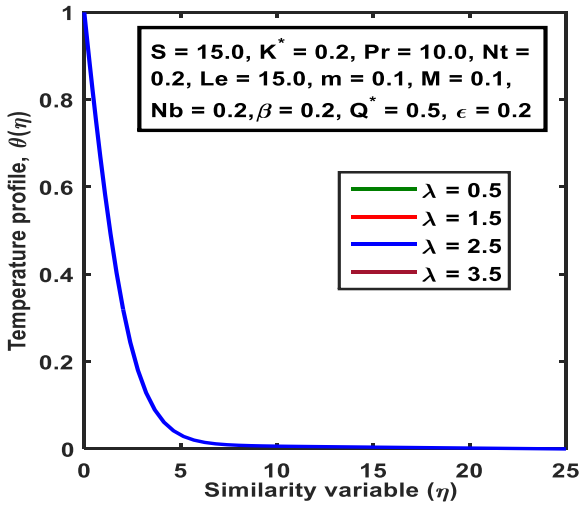

(f)

Figure 3. Temperature profile with η for the variation of (a) *Pr*, (b) *Nb*, (c) *Nt*, (d) *S* (e) Q* and (f) λ

VII. CONCENTRATION PROFILE

The influence of the Prandtl number, Lewis number (Le), Brownian motion, thermophoresis parameter, heat generation parameter, and suction parameter on the concentration profiles have been plotted in figures 4(a–f). From these figures, it is noticed that the concentration profiles and concentration boundary layer reduce by enhancing the values of Prandtl number, Lewis number, thermophoresis parameter, heat generation parameter, and suction parameter whereas the reverse trend is observed for the Brownian motion. The increasing values of the Lewis number mean reducing the mass diffusivity as a result the concentration decreases. From Figure 4(c), it is seen that the concentration boundary layer thickness decreases for an increment of the Brownian motion parameter because due to the increment of the mass transfer rate. Since the nanoparticles are moving randomly which scatter the nanoparticles quickly as a result concentration decreases. Again, the thermophoresis accelerates the fluid particles from a hotter area to a cooler area as a result particle moves quickly from the hotter region to the surrounding fluid, and therefore the concentration increases within the boundary layer.

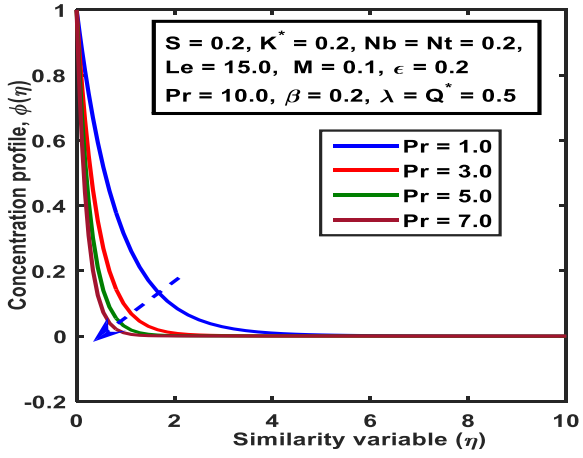

(a)

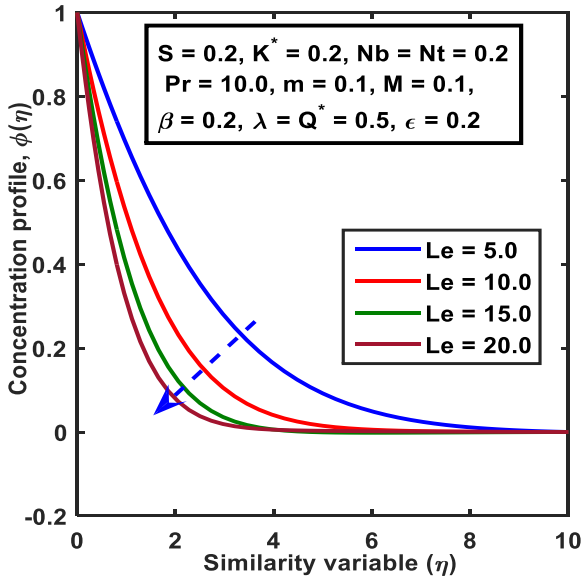

(b)

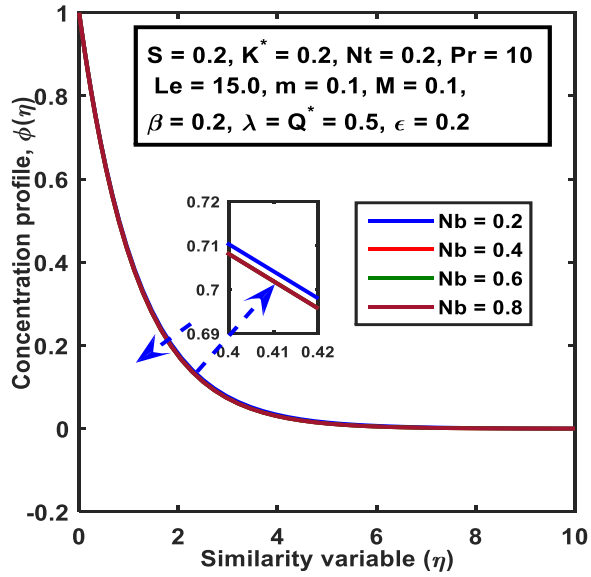

(c)

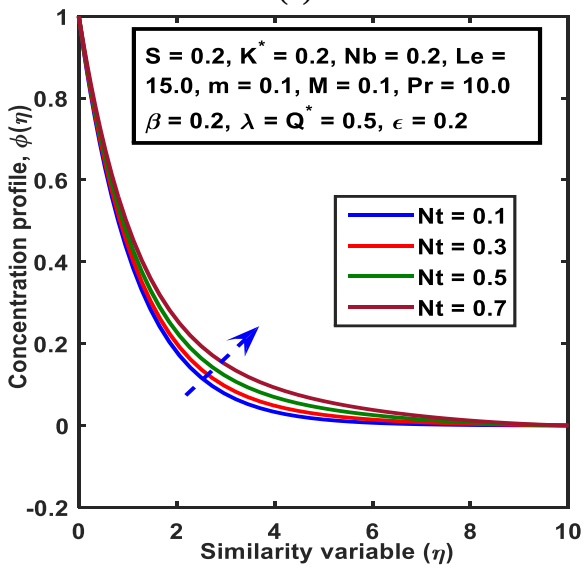

(d)

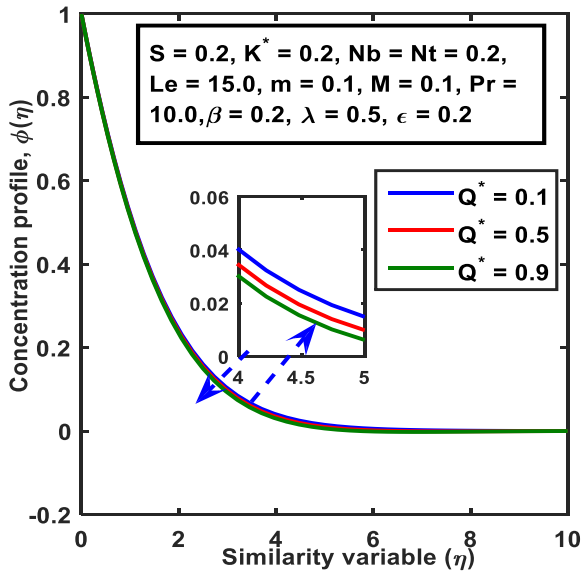

(e)

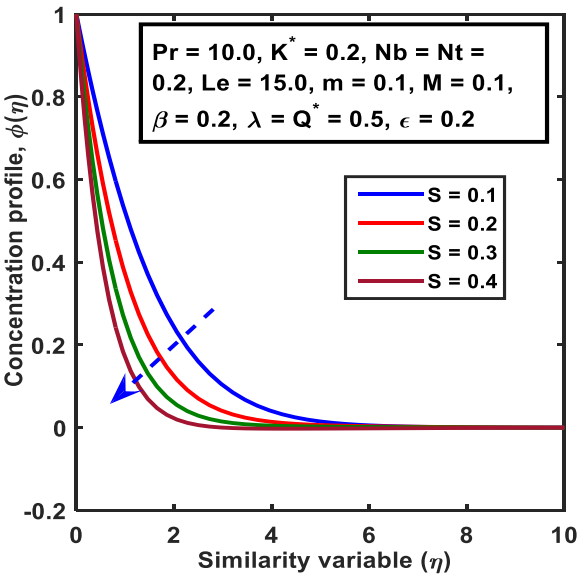

(f)

Figure 4. Concentration profile with η for the variation of (a) *Pr*, (b) *Le*, (c) *Nb*, (d) Nt (e) Q*, and (f) *S*

VIII. Skin Friction, Heat, and Mass Transfer Rate

Table 1 represents the numerical values of the skin friction which is directly proportional to velocity gradient for various values of stretching ratio parameter, porosity parameter, magnetic parameter, wedge angle parameter, mixed convection parameter, and suction parameter. From this table, it is observed that the skin friction reduces for the increasing effect of the stretching ratio parameter whereas the skin friction enhances for the increasing influence of the porosity parameter, magnetic parameter, wedge angle parameter, mixed convection parameter, and suction parameter.

Table 2 depicts the numerical values of the Nusselt and Sherwood numbers which are directly proportional to temperature and concentration gradient for various values of stretching ratio parameter, Brownian motion, thermophoresis parameter, heat generation parameter, mixed convection parameter, and suction parameter. From this table it is noticed that the Nusselt number reduces for the increasing effect of the Brownian motion, thermophoresis parameter, and heat generation parameter whereas the reverse result arises for the stretching ratio parameter, mixed convection parameter, and suction parameter. The Sherwood number reduces for the increasing effect of the thermophoresis parameter but enhances for the stretching ratio parameter, Brownian motion, heat generation parameter, mixed convection parameter, and suction parameter. The present numerical results of the heat transfer rate have been compared with Mohammadi *et al.* [3] which displays in Table 3. From this table, it is observed that the comparisons of the present numerical results show a good agreement with previously published results under the special cases. This comparison ensures the validity and accuracy of the current research work.

Table 1 Numerical values of the skin friction, for stretching ratio parameter, porosity parameter, magnetic parameter, wedge angle parameter, mixed convection parameter, and suction parameter.

ϵ	K^*	M	β	λ	S	$f''(0)$
0.0	0.5	1.0	0.2	0.5	1.0	**2.1168**
0.4	0.5	1.0	0.2	0.5	1.0	**1.3877**
0.6	0.5	1.0	0.2	0.5	1.0	**1.0014**
0.2	**2.5**	1.0	0.2	0.5	1.0	**2.0811**
0.2	**4.5**	1.0	0.2	0.5	1.0	**2.3493**
0.2	**6.5**	1.0	0.2	0.5	1.0	**2.5841**
0.2	0.5	**5.0**	0.2	0.5	1.0	**2.3493**
0.2	0.5	**10.0**	0.2	0.5	1.0	**2.8944**
0.2	0.5	**15.0**	0.2	0.5	1.0	**3.3386**
0.2	0.5	1.0	**0.2**	0.5	1.0	**1.8127**
0.2	0.5	1.0	**0.3**	0.5	1.0	**1.8599**
0.2	0.5	1.0	**0.4**	0.5	1.0	**1.8729**
0.2	0.5	1.0	0.2	**1.5**	1.0	**2.2826**
0.2	0.5	1.0	0.2	**2.5**	1.0	**2.7135**
0.2	0.5	1.0	0.2	**3.5**	1.0	**3.1312**
0.2	0.5	1.0	0.2	0.5	**0.0**	**1.3671**
0.2	0.5	1.0	0.2	0.5	**1.0**	**1.8362**
0.2	0.5	1.0	0.2	0.5	**2.0**	**2.3978**

Table 2 Computed values of Nusselt number and Sherwood number which are equivalent to the rate of heat transfer, and mass transfer for stretching ratio parameter, Brownian motion, thermophoresis parameter, heat generation parameter, mixed convection parameter, and suction parameter

ϵ	Nb	Nt	Q*	λ	S	$\lvert-\theta'(0)\rvert$	$\lvert-\varphi'(0)\rvert$
0.0	0.5	0.5	0.5	0.5	1.0	**1.0098**	**4.7049**
0.2	0.5	0.5	0.5	0.5	1.0	**1.0607**	**4.8127**
0.4	0.5	0.5	0.5	0.5	1.0	**1.1095**	**4.9164**
0.2	**0.2**	0.5	0.5	0.5	1.0	**0.6822**	**5.3913**
0.2	**0.4**	0.5	0.5	0.5	1.0	**0.4701**	**5.4288**
0.2	**0.6**	0.5	0.5	0.5	1.0	**0.2883**	**5.4424**
0.2	0.5	**0.2**	0.5	0.5	1.0	**0.6101**	**4.8382**
0.2	0.5	**0.4**	0.5	0.5	1.0	**0.3681**	**4.5073**
0.2	0.5	**0.6**	0.5	0.5	1.0	**0.2840**	**4.2814**
0.2	0.5	0.5	**0.5**	0.5	1.0	**0.6101**	**5.2622**
0.2	0.5	0.5	**0.8**	0.5	1.0	**0.4849**	**5.3842**
0.2	0.5	0.5	**1.2**	0.5	1.0	**0.2913**	**5.5725**
0.2	0.5	0.5	0.5	**1.5**	1.0	**0.6292**	**5.2933**
0.2	0.5	0.5	0.5	**2.5**	1.0	**0.6465**	**5.3227**
0.2	0.5	0.5	0.5	**3.5**	1.0	**0.6624**	**5.3506**
0.2	0.5	0.5	0.5	0.5	**0.0**	**0.1909**	**1.6484**
0.2	0.5	0.5	0.5	0.5	**1.0**	**0.6101**	**5.2622**
0.2	0.5	0.5	0.5	0.5	**2.0**	**1.1027**	**9.4395**

Table 3 Comparison of heat transfer rate for various values of Pr with β = 1/10 and other parameters are zero

	Mohammadi *et al.* [3]	Present results	Presentence of error
Pr	-θ'(0)	- θ'(0)	- θ'(0)
0.72	0.501508	0.5044	-0.6%
6.0	1.107140	1.0912	-0.0014%
10.0	1.317881	1.3215	0.3%

IX. CORRELATION COEFFICIENT ANALYSIS OF VELOCITY GRADIENT

From Table 4, it is seen that the velocity gradient is positively correlated with the parameters K*, M, S, β, and λ but negatively correlated with ϵ. Hence, the fluid velocity within the boundary layer region is negatively correlated with the parameters K*, M, S, β, and λ but positively correlated with ϵ. Table 5 represents the correlation

coefficient for the temperature gradient. It is noticed that the temperature gradient is positively correlated with the parameters K*, M, S, and ϵ but negatively correlated with Nb, Nt, and Q* respectively. Therefore, the temperature of the fluid in the boundary layer region is negatively correlated with the parameters K*, M, S, and ϵ but positively correlated with Nb, Nt, and Q* respectively. From Table 6 it is observed that the concentration gradient is positively correlated with Nb, Le, and S whereas negatively correlated with K*, M, and Nt respectively.

Table 4 Correlation coefficient of the velocity gradient

	ϵ	K*	M	β	λ	S
ϵ	1.00					
K*	-0.03	1.00				
M	-0.03	-0.07	1.00			
β	-0.02	-0.03	-0.03	1.00		
λ	-0.03	-0.07	-0.07	-0.03	1.00	
S	0.03	0.05	0.05	0.03	0.05	1.00
$f''(0)$	-0.34	0.25	0.56	0.01	0.47	0.54

Table 5 Correlation coefficient of the temperature gradient

	ϵ	K*	M	Nb	Nt	Q*	S
ϵ	1.00						
K*	-0.03	1.00					
M	-0.03	-0.07	1.00				
β	-0.02	-0.03	-0.03				
Nb	-0.02	-0.05	-0.05	1.00			
Nt	-0.03	-0.07	-0.07	-0.05	1.00		
Q*	-0.01	-0.03	-0.03	-0.02	-0.03	1.00	
S	0.03	0.05	0.05	0.04	0.06	0.02	1.00
$\theta'(0)$	0.18	0.27	0.28	-0.27	-0.38	-0.22	0.53

Table 6 Correlation coefficient of the concentration gradient

	K*	M	Nb	Nt	Le	S
K*	1.00					
M	-0.07	1.00				
Nb	-0.05	-0.05	1.00			
Nt	-0.07	-0.07	-0.05	1.00		
Le	-0.06	-0.06	-0.04	-0.07	1.00	
S	0.05	0.05	0.04	0.06	0.05	1.00
$\varphi'(0)$	-0.06	-0.05	0.02	-0.11	0.73	0.66

In Table 7 all the P – VALUE is less than 0.05. Therefore, all dimensionless parameters are statistically significant. Therefore, from Table 7 the regression model is

$$C_f\sqrt{\mathrm{Re}_x} = 1.31 - 1.98\varepsilon + 0.11M + 0.27\beta + 0.13K^* + 0.05Q^* + 0.02Nb + 0.04Nt + 0.44\lambda + 0.4S$$

So, from this model, it is observed that if we the one-unit value of mentioned parameters then we will get the average change of the skin friction.

It is observed from Table 8 that the significant parameters are K*, M, β, Nb, Nt, and Q* respectively because the P – VALUE is less than 0.05 which are highlighted in the table. So the regression model of the Nusselt number which is proportional to the temperature gradient can be written as

$$Nu_x\left(\mathrm{Re}_x\right)^{-1/2} = 1.06 + 0.64\varepsilon + 0.03M + 1.11\beta + 0.06K^* - 0.6Q^* - 0.57Nb - 0.34Nt - 0.03Le - 0.07\lambda + 0.31S$$

From the model, it is observed that if we change the one-unit value of the parameters then we will obtain the average change of the temperature gradient.

In Table 9 the significant parameters are Nt, Le, and S because the P – VALUE is less than 0.05 which are highlighted in the table. From the model, it is observed that if we change the one-unit value of the independent variables then we will obtain the average change of the dependent variable. So, from the table the regression model of the Sherwood number which is directly proportional to concentration gradient and can be written as

$$Sh_x\left(\sqrt{\mathrm{Re}_x}\right)^{-1} = -2.68 - 0.03\varepsilon - 0.02M - 0.82\beta - 0.06K^* + 0.52Q^* + 0.34Nb + 0.64Nt + 1.01Le + 0.08\lambda + 2.18S$$

X. CONCLUSIONS

Mixed convection boundary layer nanofluid flow over a stretching permeable wedge-shaped surface with magnetic effect has been investigated numerically by using the spectral quasi-linearization method with MATLAB. From the simulations, the following conclusions are summarized.

- The fluid velocity within the boundary layer region is negatively correlated with the parameters K*, M, S, β, and λ but positively correlated with ϵ.
- The temperature gradient is positively correlated with the parameters K*, M, S, and ϵ but negatively correlated with Nb, Nt, and Q* respectively. Therefore, the temperature of the fluid in the boundary layer region is negatively correlated with the parameters K*, M, S, and ϵ but positively correlated with Nb, Nt, and Q* respectively.
- The concentration gradient is positively correlated with Nb, Le, and S whereas negatively correlated with K*, M, and Nt respectively.
- The skin friction coefficient increases about 42%, 3.3%, 37.2%, 75.4% and 24.2% due to increasing stretching ratio parameter (0.0 to 0.6), magnetic parameter (5.0 to 15.0), wedge angle parameter (36^0 to 72^0), mixed convection parameter (1.5 to 3.5), suction parameter (0.0 to 2.0) and porosity parameter (2.5 to 6.5), respectively. On the other hand, increasing the

stretching ratio parameter (0 to 0.4) decreases the skin friction by 52.7%.

- increasing values of stretching ratio parameter (0.0 to 0.4), mixed convection parameter (1.5 to 3.5) and suction parameter (0 to 2.0) increase the heat transfer rate by approximately 1.2%, 5.1% and 477%, respectively but Brownian motion (0.2 to 0.6), thermophoresis (0.2 to 0.6) and heat generation parameter (0.5 to 1.2) decrease the heat transfer rate by 32.3%, 53.5%, and 52.3%, respectively.
- Rate of mass transfer enhances about 4.5%, 0.9%, 5.9%, 1.2%, and 472.6% for changing stretching ratio parameter 0.0 to 0.4, Brownian motion 0.2 to 0.6, heat generation parameter 0.5 to 1.2, mixed convection parameter 1.5 to 3.5 and suction parameter 0.0 to 2.0 but reduces 11.5% when thermophoresis parameter changes 0.2 to 0.6.

A. Abbreviations and Acronyms

MHD	magnetohydrodynamic
α	base fluid thermal diffusivity, m^2s^{-1}
K	permeability, m^2
g	acceleration due to gravity, ms^{-2}
σ	electrical conductivity, sm^{-1}
D_B	coefficient of Brownian motion, cm^2s^{-1}
D_T	coefficient of thermophoresis
v	fluid kinematics viscosity, m^2s^{-1}
ρ	fluid density, kg m^{-3}
B_0	strength of the magnetic field, Am^{-1}
u	velocity component, ms^{-1}
Ω	total wedge angle
a	initial stretching constant
β	wedge angle parameter
M	magnetic parameter
S	suction parameter
m	power-law index parameter
Nb	Brownian motion
C_f	skin friction coefficient
Sh_x	local Sherwood number
PDEs	partial differential equations
ODEs	ordinary differential equations
BL	boundary layer
SQLM	spectral quasi-linearization method
v	y-axis velocity component, ms^{-1}
U	free stream velocity
τ	the ratio of the effective heat capacity
ϵ	stretching ratio parameter
C	nanoparticle concentration, kg m^{-3}
C_w	surface concentration, kg m^{-3}
C_∞	free stream concentration
T	fluid temperature, k^{-1}
^Tw	surface temperature, k^{-1}
T_∞	free stream temperature
ψ	stream function
η	similarity variable
b	free stream constant
K^*	permeability parameter
Nt	thermophoresis parameter
Le	Lewis number
Pr	Prandtl number
Re_x	Reynolds number
Gr	Grashof number
λ	mixed convection parameter
Nu_x	local Nusselt number
Sh_x	local Sherwood number
β^*	coefficient of thermal expansion
γ	stream function
$f(\eta)$	dimensionless stream function
$f'(\eta)$	dimensionless velocity
$\theta(\eta)$	dimensionless temperature
$\varphi(\eta)$	dimensionless concentration
C_F	Skin friction coefficient

REFERENCES

[1] V. M. Falkner, and S. W. Skan, "Some approximate solutions of the boundary layer equations", *Philosophical Magazine*, **Vol. 12, pp. 865–896, 1931.**

[2] V. Nagendramma, K. Sreelakshmi, and G. Sarojamma, "MHD heat and mass transfer flow over a stretching wedge with convective boundary condition and thermophoresis", *Science Direct, Proceedia Eng.*, **Vol. 127, pp. 963–96, 2015.**

[3] F. Mohammadi, M. M. Hosseini, A. Dehgahn, and F. M. Ghaini, "Numerical Solutions of Falkner-Skan Equation with Heat Transfer Studies", *Nonlinear Science,* **Vol. 3, pp. 86-93, 2012.**

[4] G. Ashwini, and A. T. Eswara, "Unsteady MHD accelerating flow past a wedge with thermal radiation and internal heat generation/absorption", *International Journal of Mathematics and Computer Science*, **Vol. 1, pp. 13-26, 2015.**

[5] B. K. Ramesh, R. K. Shreenivas, L. N. Achala and N. M. Bujurke, "Similarity solutions of the MHD boundary layer flow past a constant wedge within porous media," *Mathematical Problems in Engineering,* **Vol. 2017, pp. 11 pages, 2017.**

[6] W. Ibrahim and A. Tulu, "Magnetohydrodynamic (MHD) boundary layer flow past a wedge with heat transfer and viscous effects of nanofluid embedded in porous media", *Mathematical Problems in Engineering,* **Vol. 2019, pp. 12, 2019.**

[7] A. Nageeb, H. Haroun, S. Mondal and P. Sibanda, "Effects of thermal radiation on mixed convection in a MHD nanofluid flow over a stretching sheet using a spectral relaxation method," *International Journal of Mathematics and Computational Sciences,* **Vol. 11, no. 2, pp. 1-10, 2017.**

[8] R. M. Kasmani, S. Sivasankaran, M. Bhuvaneswari, A. K. Hussein, "Analytical and numerical study on convection of nanofluid past a moving wedge with soret and dufour effects", *International Journal of Numerical Methods Heat and Fluid Flow,* **Vol.27, pp. 2333-2354, 2017.**

[9] I. Waini, A. Ishak, and I. Pop, "MHD flow and heat transfer of a hybrid nanofluid past a permeable stretching/shrinking wedge", *Applied Mathematical Mechanics,* **Vol. 41, pp. 507–520, 2020.**

[10] Rajab Al-Sayagh, Control of the free convective heat transfer using a U-shaped obstacle in an Al2O3-water nanofluid filled cubic cavity, *International Journal of Advanced Applied Science*, **Vol. 8, pp. 23-30, 2021.**

[11] J. Buongiorno, "Convective transport in nanofluids", *ASME Journal of Heat Transfer,* **Vol. 128, pp. 240–250, 2006.**

[12] W. A. Khan, and I. Pop, "Boundary layer flow past a wedge moving in a nanofluid", *Mathematical Problem in Engineering,* **Vol. 1, 2013.**

[13] R. E. Bellman, and R. E. Kalaba, "Quasilinearization and Nonlinear Boundary-Value Problems", *Elsevier, New York, NY, USA,* 1965.

[14] Y. Menni, A. J. Chamkha, N. Massarotti, H. Ameur, N. Kaid, and M. Bensafi, "Hydrodynamic and thermal analysis of water, ethylene glycol and water-ethylene glycol as base fluids dispersed by aluminum oxide nano-sized solid particles", *International Journal of Numerical Methods for Heat & Fluid Flow,* **Vol. 30, pp. 4349-4386, 2020.**

[15] A. A. Khan, K. Zaimi, S. F. Sufahani, and M. Ferdows, "MHD Flow and Heat Transfer of Double Stratified Micropolar Fluid over a Vertical Permeable Shrinking/Stretching Sheet with Chemical Reaction and Heat Source", *Journal of Advanced Research in Applied Sciences and Engineering Technology,* **Vol. 21, pp. 1–14, 2020.**

[16] N. S. Yusof, S. K. Soid, M. R. Illias, A. S. Abd Aziz, and N. A. A. Mohd Nasir, "Radiative Boundary Layer Flow of Casson Fluid Over an Exponentially Permeable Slippery Riga Plate with Viscous Dissipation", *Journal of Advanced Research in Applied Sciences and Engineering Technology,* **Vol. 21, pp. 41–51. 2020.**

[17] K. M. Ewis, "Effects of Variable Thermal Conductivity and Grashof Number on Non-Darcian Natural Convection Flow of Viscoelastic Fluids with Non-Linear Radiation and Dissipations", *Journal of Advanced Research in Applied Sciences and Engineering Technology,* **Vol. 22, pp. 69–80, 2021.**

[18] A.O. Nyakebogo, J.M. Kerongo, R.K. Obogi, "Stability and Consistency Analysis of FTCS Scheme for Unsteady Magnetohydrodynamic Fluid Flow over a Vertical Stretching Sheet," *International Journal of Scientific Research in Mathematical and Statistical Sciences,* **Vol.8, Issue.4, pp.41-46, 2021.**

[19] R. Mehta, H. R. Kataria, "Magnetic Field a Heat Generation Effects on Second Grade Fluid Flow past an Oscillating Vertical Plate in Porous Medium," *International Journal of Scientific Research in Mathematical and Statistical Sciences,* **Vol.7, Issue.2, pp.1-8, 2020.**

[20] J. Wilfred Samuel Raj, S.P. Anjali Devi, "Numerical analysis of nonlinear radiation, viscous and Ohmic dissipation effects on steady Magnetohydrodynamic forced convection flow over a shrinking surface with internal heat generation/absorption," *International Journal of Scientific Research in Mathematical and Statistical Sciences,* **Vol.7, Issue.2, pp.9-6, 2020.**

AUTHORS PROFILE

Mr. Mohammad Ali pursed Bsc. Hons., M. Phil., and Ph. D.(running) Applied Science from CU, Chittagong, BUET, Dhaka in 2002, 2002 & 2009. He is currently working as Associate Professor in Department of Mathematics from CUET, Chittagong since 2002. He is a life member of Mathematical Society since 2003, and Life member of Bangladesh Academy of Science since 2016. He has published more than 52 research papers in reputed international journals including Scopus index (SCI & Web of Science) and conferences including IEEE, AIP, Preceedia engineering and it's also available online. His main research work focuses on boundary flow with heat and mass transfer, Optimization, and Computational Mathematics. He has 19 years of teaching experience and 08 years of research experience.

Table 7. Regression analysis for the parameters *M, m* Pr, *Q*, Ec, λ,* and ϵ and the local skin friction coefficient ($C_f\sqrt{\mathrm{Re}_x}$) by taking 1st order coefficient.

SUMMARY OUTPUT						
Regression Statistics						
Multiple R	1.00					
R Square	0.99					
Adjusted R Square	0.99					
Standard Error	0.05					
Observations	41.00					
ANOVA						

	df	SS	MS	F	Significance F	
Regression	10.00	10.16	1.02	364.47	0.00	
Residual	30.00	0.08	0.00			
Total	40.00	10.24				
	Coefficients	Standard Error	t Stat	P-value	Lower 95%	Upper 95%
Intercept	1.31	0.08	15.76	0.00	1.14	1.48
ϵ	-1.98	0.11	-18.11	0.00	-2.20	-1.76
K*	0.13	0.01	17.24	0.00	0.11	0.14
M	0.11	0.00	34.65	0.00	0.11	0.12
β	0.27	0.22	1.22	0.23	-0.18	0.71
Nb	0.02	0.05	0.38	0.71	-0.08	0.11
Nt	0.04	0.02	1.92	0.06	0.00	0.08
Le	0.00	0.01	0.34	0.74	-0.01	0.01
Q*	0.05	0.06	0.79	0.44	-0.08	0.18
λ	0.44	0.01	29.59	0.00	0.41	0.47
S	0.40	0.01	28.44	0.00	0.37	0.43

Table 8 Regression analysis for the parameters ϵ, K*, M, β, Nb, Nt, Q*, Le, λ, and S with local Nusselt number $Nu_x \left(\mathrm{Re}_x\right)^{-1/2}$ by taking 2nd order coefficient.

Regression Statistics						
Multiple R	0.87					
R Square	0.76					
Adjusted R Square	0.68					
Standard Error	0.19					
Observations	41.00					
ANOVA						
	df	SS	MS	F	Significance F	
Regression	10.00	3.51	0.35	9.33	0.00	
Residual	30.00	1.13	0.04			
Total	40.00	4.64				
	Coefficients	Standard Error	t Stat	P-value	Lower 95%	Upper 95%
Intercept	1.06	0.30	3.49	0.00	0.44	1.69
ϵ	0.64	0.40	1.60	0.12	-0.18	1.46
K*	0.06	0.03	2.10	0.04	0.00	0.11
M	0.03	0.01	2.22	0.03	0.00	0.05
β	1.11	0.80	1.39	0.18	-0.53	2.75
Nb	-0.57	0.17	-3.32	0.00	-0.92	-0.22
Nt	-0.34	0.08	-4.47	0.00	-0.50	-0.18
Le	-0.03	0.02	-1.61	0.12	-0.08	0.01

Q*	-0.60	0.23	-2.65	0.01	-1.07	-0.14
λ	-0.07	0.05	-1.33	0.19	-0.18	0.04
S	0.31	0.05	6.06	0.00	0.21	0.42

Table 9. Regression analysis for the independent parameters ϵ, K*, *M, β, Nb, Nt, Q*, Le, λ*, and F_w with Sherwood number $Sh_x\left(\sqrt{\mathrm{Re}_x}\right)^{-1}$ by taking 2nd order coefficient.

Regression Statistics						
Multiple R	0.97					
R Square	0.94					
Adjusted R Square	0.92					
Standard Error	0.59					
Observations	41.00					
	df	SS	MS	F	Significance F	
Regression	10.00	169.58	16.96	49.54	0.00	
Residual	30.00	10.27	0.34			
Total	40.00	179.85				
	Coefficients	Standard Error	t Stat	P-value	Lower 95%	Upper 95%
Intercept	-2.68	0.92	-2.91	0.01	-4.55	-0.80
ϵ	-0.03	1.21	-0.03	0.98	-2.50	2.44
K*	-0.06	0.08	-0.77	0.45	-0.23	0.10
M	-0.02	0.04	-0.69	0.49	-0.10	0.05
β	-0.82	2.42	-0.34	0.74	-5.77	4.13
Nb	0.34	0.52	0.66	0.51	-0.71	1.40
Nt	0.64	0.23	2.80	0.01	0.17	1.11
Le	1.01	0.06	15.92	0.00	0.88	1.14
Q*	0.52	0.69	0.76	0.46	-0.88	1.92
λ	0.08	0.16	0.50	0.62	-0.25	0.42
S	2.18	0.16	13.93	0.00	1.86	2.50

